Journal of Peptide Science
J. Pept. Sci. 2008; **14**: 139–151
Published online 21 December 2007 in Wiley InterScience (www.interscience.wiley.com). DOI: 10.1002/psc.978

JOURNAL OF PEPTIDE SCIENCE

Ranking the affinity of aromatic residues for carbon nanotubes by using designed surfactant peptides‡

HUI XIE,[a,b] ERIC J. BECRAFT,[a] RAY H. BAUGHMAN,[a,b] ALAN B. DALTON[c] and GREGG R. DIECKMANN[a,b]*

[a] Department of Chemistry, The University of Texas at Dallas, 2601 North Floyd Road, Richardson, Texas, 75083-0688, USA
[b] NanoTech Institute, The University of Texas at Dallas, 2601 North Floyd Road, MS BE26, Richardson, Texas, 75083-0688, USA
[c] Department of Physics, University of Surrey, Guildford GU2 7XH, UK

Received 10 July 2007; *Revised 16 October 2007*; *Accepted 22 October 2007*

Abstract: A series of surfactant peptides were created to evaluate the affinity of aromatic AAs for single-walled carbon nanotubes in the absence of complications from peptide folding or self-association. Each surfactant peptide has a lipidlike architecture, with two Lys residues at the *C*-terminus as a hydrophilic head, five Val residues to form a hydrophobic tail, and the testing AA at the *N*-terminus. Raman and CD spectroscopic studies reveal that the surfactant peptides have a large unordered structural component which is independent of peptide concentration, suggesting that the peptides undergo minimal association under experimental conditions, thus removing this interference from interpretation of the peptide/carbon nanotube interactions. A lack of peptide self-association is also indicated by sedimentation equilibrium ultracentrifugation results. Optical spectroscopy of the peptide/carbon nanotube dispersions indicate that among the three aromatic AAs, tryptophan has the highest affinity for carbon nanotubes (both bundled and individual states) when incorporated into a surfactant peptide, while the Tyr-containing peptide is more selective for individual carbon nanotubes. Phe has the lowest overall affinity for carbon nanotubes. Raman spectra of dispersions made with SPF, SPY and SPW display similar types of nanotubes dispersed, although differences in the relative nanotube populations are observed by optical spectroscopy. Copyright © 2007 European Peptide Society and John Wiley & Sons, Ltd.

Keywords: nanotechnology; protein design; carbon nanotube; dispersion; surfactant; Raman spectroscopy; sedimentation equilibrium ultracentrifugation; aromatic residue

INTRODUCTION

Carbon nanotubes possess extraordinary physical and mechanical properties because of their ordered, one-dimensional structures. A CNT is a seamless cylinder formed from the rolling of a single sheet of graphite with diameters that vary between 0.5 and 5 nm and a range of lengths that can exceed 1 μm [1]. Depending on the spiral arrangement of the hexagonal rings in the graphite and the diameter of the resulting cylinder, CNTs can be either semiconductors or metallic in nature. A great deal of attention has been focused on this novel nanoscale material, and a variety of potential applications of CNTs have been proposed [1]. However, many of these research activities have been hampered by the fact that as-synthesized CNTs lack dispersability in aqueous solution because of their hydrophobic surfaces [2]. Currently, the strategies employed in dispersing CNTs can be divided into two categories. One group of processes involves chemical functionalization, or the covalent attachment of solubilizing moieties to the surface of the CNTs [3–7]. Although effective at enhancing the solubility of CNTs, this approach disrupts the sp^2 hybridization of the carbon atoms, consequently changing the inherent properties of the CNTs [8,9]. Another dispersal method that preserves the properties of the CNTs is the noncovalent coating of CNTs with surfactant molecules [10,11], conjugated polymers [12–14] or biological macromolecules [15,16].

Small designed peptides present another exciting method for the noncovalent dispersion of CNTs [17,18]. Previous work from our group has demonstrated that designed amphiphilic α-helical peptides are excellent at dispersing SWNTs [19–23]. The basic design of the helical peptides makes use of a (Val-*b*-*b*-X-*b*-*b*-*b*) heptad repeat [24], where X is an aromatic AA (Phe, Tyr or Trp) and *b* typically represents more polar AAs. Once the peptide is folded into a helical secondary structure, an amphiphilic architecture is achieved. The aromatic AAs in the sequence lead to strong interactions with the SWNT hydrophobic surface via π-stacking [23,25,26], with more aromatic AAs resulting in improved dispersion of SWNTs.

Amphiphilic helical peptides are also capable of self-associating into helical aggregates [27–29]. The fact

Abbreviations: SPK, surfactant peptide containing a Lys; SPF, surfactant peptide containing a Phe; SPW, surfactant peptide containing a Trp; SPY, surfactant peptide containing a Tyr; CNT, carbon nanotube; SWNT, single-walled CNT; AA, amino acid; SEM, Scanning Electron Microscopy; RBM, radial breathing mode.

* Correspondence to: Gregg R. Dieckmann, Department of Chemistry, The University of Texas at Dallas, 2601 North Floyd Road, MS BE26, Richardson, Texas, 75083-0688, USA; e-mail: dieckgr@utdallas.edu
‡ This article is part of the Special Issue of the Journal of Peptide Science entitled "Peptides in Nanotechnology".

that these peptides both fold and self-associate complicates efforts to evaluate the strength of peptide/SWNT interactions and design more effective SWNT dispersal agents. What is needed is a simple model system that will allow easy analysis of the interactions between a particular AA and SWNTs in the absence of complicating factors like peptide aggregation or folding. In the present work, we have designed a series of surfactant peptides to compare the interactions between different aromatic AAs and SWNTs. These eight-residue peptides, each approximately 2 nm in length, have a lipidlike architecture, with two Lys residues at the *C*-terminus as a hydrophilic head, five Val residues to form a hydrophobic tail, and the testing aromatic AA at the *N*-terminus (Figure 1). We first demonstrate that the surfactant peptides display minimal folding and self-association properties under the experimental conditions used to disperse CNTs. We then investigate the ability of different peptides to form SWNT dispersions and show that various surfactant peptides differ in their abilities to disperse SWNTs. SPW, the peptide containing Trp, is best at dispersing SWNTs in both bundled and individual states. The peptide containing Tyr (SPY) is more selective for individual SWNTs.

MATERIALS AND METHODS

Peptide Synthesis and Purification

The peptides, which contain the AA sequence Ac-X$(Val)_5$ LysLys-$CONH_2$ (Ac indicates *N*-terminal acetylation, $CONH_2$ indicates *C*-terminal amidation, and X indicates the testing AA), were synthesized and purified following previously published methods [19].

Peptide/SWNT Sample Preparation

Unpurified SWNTs produced by the method of high-pressure disproportionation of carbon monoxide (HiPco process) were obtained from Carbon Nanotechnologies, Inc. (lot # R0223). Solutions of 100 μM peptide were prepared using D_2O or H_2O, with peptide concentrations determined by UV–Vis absorption spectrometry using the absorbance of the peptide chromophore (Phe: $\varepsilon_{257} = 197\ cm^{-1}\ M^{-1}$; Trp: $\varepsilon_{280} = 5600\ cm^{-1}\ M^{-1}$; Tyr: $\varepsilon_{275} = 1420\ cm^{-1}\ M^{-1}$) or estimated by mass (for SPK). For each sample, a 1.0 ml volume of 100 μM peptide was added into a plastic 1.5-ml Eppendorf tube containing HiPco SWNTs (0.75–1.50 mg), and the mixture was then vortexed for approximately 1 min. Sonication was performed using a VWR Scientific Branson Sonifier 250-horn sonicator with the peptide/SWNT sample immersed in an ice–water bath, and the 2-mm diameter tip placed into the sample at approximately one-third of the distance from the surface. Samples were sonicated for 4 min at a power level of 10 W, yielding dense black mixtures. The sonicated samples were first centrifuged in an Eppendorf 5417C centrifuge for 10 min at 16 000 *g*. The upper 75% of the supernatant was then recovered using a small-bore pipet, avoiding sedimentation at the bottom. The supernatant was then transferred to a Beckman centrifuge tube and centrifuged for 120 min at 100 000 *g* and 4 °C in a Beckman TL-100 ultracentrifuge. The upper 50% of the supernatant was recovered using a small-bore pipet, avoiding sedimentation at the bottom, and transferred to a clean tube, yielding homogeneous gray dispersions. For peptide/SWNT dispersion concentration studies, the samples were prepared in deionized water (DI) and centrifuged twice for 10 min with each spin at 16 000 *g*.

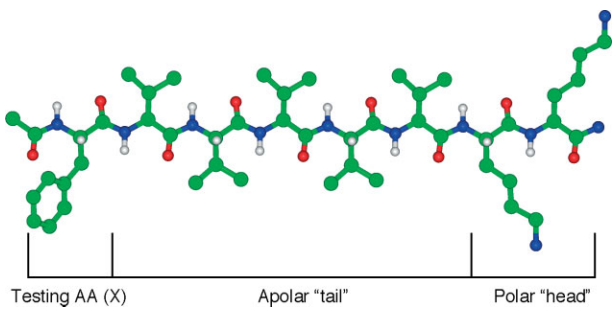

Figure 1 Ball-and-stick schematic representation of the surfactant peptide SPF. Substitution of Trp, Tyr and Lys for the testing AA generates the other peptides SPW, SPY and SPK, respectively [atom colors: green, carbon; blue, nitrogen; red, oxygen; white, hydrogen]. Hydrogen atoms have been removed from the side chains for clarity.

CD Spectroscopy

CD spectral measurements were made at 25 °C using an Aviv model 202 CD spectrophotometer and 1-mm path length rectangular quartz cuvettes. Spectra were collected from 190 to 260 nm at 1-nm intervals and an averaging time of 5 s at each wavelength step. The CD signal was converted to mean residue ellipticity ($[\theta]$, deg cm^2 $dmol^{-1}$) using Eqn (1):

$$[\theta] = \frac{S_{obs}}{10 \times l \times c \times n} \quad (1)$$

where S_{obs} is the corrected CD signal (millidegrees), l is the pathlength of the cell (cm), c is the peptide concentration (mol l^{-1}) and n is the number of AAs per peptide. CD data were analyzed for secondary structure composition using the deconvolution software CDPro [30].

Optical Spectroscopy

Absorption spectra of peptide/SWNT dispersions were obtained using a Perkin-Elmer Lamda 900 UV–Vis–NIR (UV–visible–near-infrared) spectrophotometer. For samples prepared in D_2O, spectra were collected from 400 to 1600 nm at 1-nm intervals. For samples prepared in DI water, spectra were collected from 400 to 1000 nm.

Raman Spectroscopy

Peptide solutions were prepared as above with the exception that the concentrated stock solutions were generated (~2 mM) and then diluted to the desired concentrations. Peptide spectra were collected on both solid and liquid samples. Each solid sample (peptide and peptide/SWNT dispersion) was prepared by dropping a stock solution onto a SpectRim Substrate (Tienta Sciences, Inc., Indianapolis, IN) and desiccating for

DOI: 10.1002/psc

~30 min prior to spectra acquisition. Each liquid sample was loaded into a 200 – μl glass cylinder, with spectra collected by focusing the laser inside the cylinder. Raman spectra were recorded on a Jobin Yvon Horiba high-resolution LabRam Raman microscope system. The laser excitations used were 633 nm and 488 nm output. The laser power at the sample was ~8 mW and was focused to ~1 μm. Wavenumber calibration was carried out using the 520.5-cm^{-1} line of the silicon wafer. Peptide spectra were recorded by scanning the 800–1800 cm^{-1} region with a total acquisition time of 60 min, and the spectra of peptide/SWNT dispersions were recorded by scanning the 50–3000 cm^{-1} region with a total acquisition time of 8 min. A spectral resolution of ~1 cm^{-1} was used. Spectra were fitted with Lorentzian functions by searching for the minimum number of frequencies that fit the different bands equally well without fixing the positions and widths of the individual peaks.

Scanning Electron Microscopy

SEM images were acquired using a LEO 1530 field-emission scanning electron microscope with accelerating voltages of either 1 or 20 keV. One drop of the 100 000 *g* peptide/SWNT dispersion was placed on a precleaned aluminum foil substrate and then dried in the air. No metal coating was used for the samples.

Sedimentation Equilibrium Ultracentrifugation

Sedimentation equilibrium studies were performed on a Beckman XL-I analytical ultracentrifuge equipped with interference optics and an An-60 Ti rotor (Beckman Instruments, Palo Alto, CA). Sample data were collected at 20 °C at three rotor speeds (20 000, 30 000 and 40 000 rpm) for each peptide (100 μM) in the absence of SWNTs. The resulting data for each peptide were globally fit using the software package Igor Pro (WaveMetrics, Inc.) to two different models: (i) a single homogeneous species model using Eqn (2):

$$S(r) = S(r_0)\exp[HM(r^2 - r_0^2)] + E \quad (2)$$

where $S(r)$ is the experimentally observed signal in fringes at radius r, $S(r_0)$ is the signal at reference radius r_0, $H = (1 - \upsilon\rho)(\omega^2/2RT)$ (where υ is the partial specific volume of the peptide, ρ is the solvent density, ω is the angular velocity in rad s^{-1}, R is the gas constant, and T is the temperature in K), M is the molecular mass, and E is the baseline offset; and (ii) a monomer/nmer equilibrium model using Eqn (3):

$$S(r) = S(r_0)\exp[HM(r^2 - r_0^2)] + \frac{nS(r_0)^n}{K_{d(n,1)}}\exp[HnM(r^2 - r_0^2)] + E \quad (3)$$

where $K_{s(n,1)}$ is the dissociation constant, and n is the Hill Coefficient (describes the association state of a peptide). The partial specific volume (ml g^{-1}) for each peptide (SPK, 0.8425; SPF, 0.8339; SPW, 0.8253; SPY, 0.8221) was calculated from the peptide composition [31,32]. The solvent density (0.99707 g ml^{-1}) was calculated using the program SEDNTERP [32].

RESULTS AND DISCUSSION

CD Spectroscopy of Surfactant Peptides in Solution

Each surfactant peptide (Figure 1) has an eight-residue amphiphilic sequence, consisting of two Lys residues at the *C*-terminus to provide a hydrophilic head, five Val residues, and one testing AA at the *N*-terminus. The *C*-terminus was amidated and the *N*-terminus acetylated for each peptide. The testing AAs are Phe, Trp and Tyr, with the corresponding peptides named SPF, SPW and SPY, respectively. A control peptide (SPK) was also synthesized, which has a Lys as the testing AA.

Amphiphilic peptides can interact with each other and, in some cases, self-assemble into nano-structured materials. In order to understand the interactions between a peptide and SWNTs, it is optimal to conduct experiments under conditions where peptide/peptide interactions are minimized. In the case where protein folding is coupled to protein self-association, monitoring the folding of the protein can be utilized to study aggregation. Therefore, the secondary structures of the surfactant peptides in the absence of CNTs were first studied as a function of peptide concentration and monitored by CD. The CD spectra of all the peptides show identical behavior; at concentrations ranging from 50 to 200 μM, the CD spectra are largely unchanged with a strong negative feature at ~200 nm and a weaker negative band around 220 nm, suggesting that each peptide contains primarily a random coil structure at concentrations below 200 μM (Figure 2). The CD data were further analyzed using CDPro [30], a suite of CD analysis programs that compares a CD spectrum to reference spectra of structurally characterized proteins to predict the secondary structure content of the polypeptide in question. The results of the CDPro analysis, presented in Table 1, also suggest that each surfactant peptide contains a mix of secondary structures at all concentrations measured, with the primary single feature being unordered structure.

Raman Spectroscopy of Surfactant Peptides in Solution and Solid State

We also utilized Raman spectroscopy to characterize the structure of the surfactant peptides both in the solid and liquid states. Peaks in the amide I region (1600–1700 cm^{-1})of polypeptides (Table 2) can be correlated with the specific secondary structures they adopt [33,34]. Figure 3 displays the amide I region of the Raman spectra for the liquid samples at a peptide concentration of 500 μM. The higher peptide concentration was used, because 100 μM samples gave signals too weak to analyze. All liquid spectra are similar, characterized by a broad band between 1612 and 1618 cm^{-1} and a sharp more intense band at 1648 cm^{-1}. The broad band at 1618 cm^{-1} in SPK is consistent with the amide I for β-sheet structure

DOI: 10.1002/psc

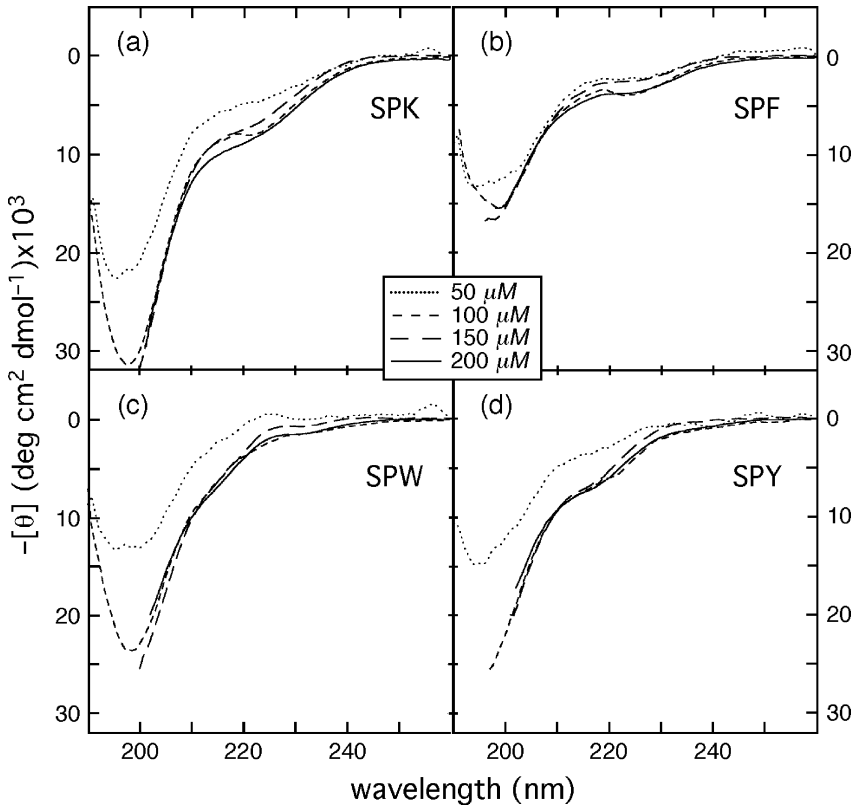

Figure 2 CD spectra of SPK (a), SPF (b), SPW (c) and SPY (d) in the absence of CNTs as a function of peptide concentration.

Table 1 Results from CDPro analysis of CD spectra for the surfactant peptides

Peptide	[peptide] (μM)	% Ordered[a] (helix/sheet/turn)	% Unordered[a]
SPK	50	58 ± 1	42 ± 1
	100	54 ± 8	46 ± 3
	150	52 ± 7	48 ± 7
	200	58 ± 12	42 ± 12
SPF	50	64 ± 2	36 ± 2
	100	58 ± 2	42 ± 2
	150	56 ± 2	44 ± 2
	200	62 ± 1	38 ± 1
SPW	50	61 ± 4	39 ± 4
	100	58 ± 1	42 ± 1
	150	56 ± 1	44 ± 1
	200	60 ± 3	40 ± 3
SPY	50	64 ± 0	36 ± 1
	100	59 ± 7	41 ± 7
	150	61 ± 5	39 ± 5
	200	64 ± 6	36 ± 6

[a] Average result from two algorithms (CONTINLL and SELCON3) in the CDPro software. For details, see Ref. 30.

(either parallel or antiparallel architectures) [35–38]. In addition, the side chains of aromatic residues often have ring-mode signals between 1600 and 1620 cm^{-1} [38–44]. Therefore, the broad band below 1620 cm^{-1} in SPF, SPW and SPY likely contains a contribution from such a ring-mode signal which shifts the broad band in these spectra to a slightly smaller frequency. Unfortunately, the signal-to-noise (S/N) ratio for the liquid samples is low enough that we are unable to resolve the amide I and ring-mode components in the broad signal. The sharp band at 1648 cm^{-1} falls in the amide I region that is often assigned to the α-helical structure [33,34], although there are a number of reports correlating a band between 1640 and 1648 cm^{-1} to an unordered or random secondary structure [38,45]. On the basis of our solution-CD results, which suggest that all surfactant peptides have a mixture of secondary structures with the primary one being random structure, we are unable to make a definitive assignment of this band to one of these options.

Figure 4 displays the amide I region of the Raman spectra for solid samples of the surfactant peptides. Although the liquid samples are more important for correlation with the CD results, solid samples, where the peptide solutions were dried on a surface, have higher local concentrations and so are amenable to the collection of Raman spectra with better S/N ratios. A *caveat*, however, is that the dried samples may show effects of peptide aggregation. The solid spectra are again similar for the peptides, with a large band located at 1665 cm^{-1} and a weaker band between 1602 and 1612 cm^{-1}. A signal at 1665 cm^{-1}

DOI: 10.1002/psc

Table 2 Assigned Raman bands in the 1600–1700 cm^{-1} amide I region (peptide only samples)

Sample	ν (cm^{-1})[a]	% Total Area[b]	Assignment
Liquid samples			
SPK	1618 (b)	70.4	β-sheets (parallel/antiparallel) [35–38]
	1648 (sh)	21.2	α-helix [33,34]; unordered [38,45]
	1665	8.4	unordered or turns [33,34,64]
SPF	1612 (b)	63.2	β-sheets (antiparallel) [36–38]; Phe side chain [41,42,44]
	1648 (sh)	36.8	α-helix [33,34]; unordered [38,45]
SPW	1612 (b)	69.3	β-sheets (antiparallel) [36–38]; Trp side chain [42–44]
	1648 (sh)	30.7	α-helix [33,34]; unordered [38,45]
SPY	1614 (b)	65.0	β-sheets (antiparallel) [36,37]; Tyr side chain [38–40,42,44]
	1648 (sh)	35.0	α-helix [33,34]; unordered [38,45]
Solid samples			
SPK	ND[c]	ND	
SPF	1602	14.7	Phe side chain [39,40,42]
	1635 (w)	6.1	β-pleated sheet [65–67]
	1665	79.2	Unordered or turns [33,34,64]
SPW	1603 (b)	49.3	Trp side chain [42]
	1647	13.5	α-helix [33,34]; unordered [38,45]
	1665	37.2	Unordered or turns [33,34]
SPY	1612	24.2	β-sheets (antiparallel) [36–38]; Tyr side chain [38–40,42]
	1665	75.8	Unordered or turns [33,34,64]

[a] b, broad; sh, sharp; w, weak.
[b] Based on fitting of spectra; see Materials and Methods for details.
[c] Not determined.

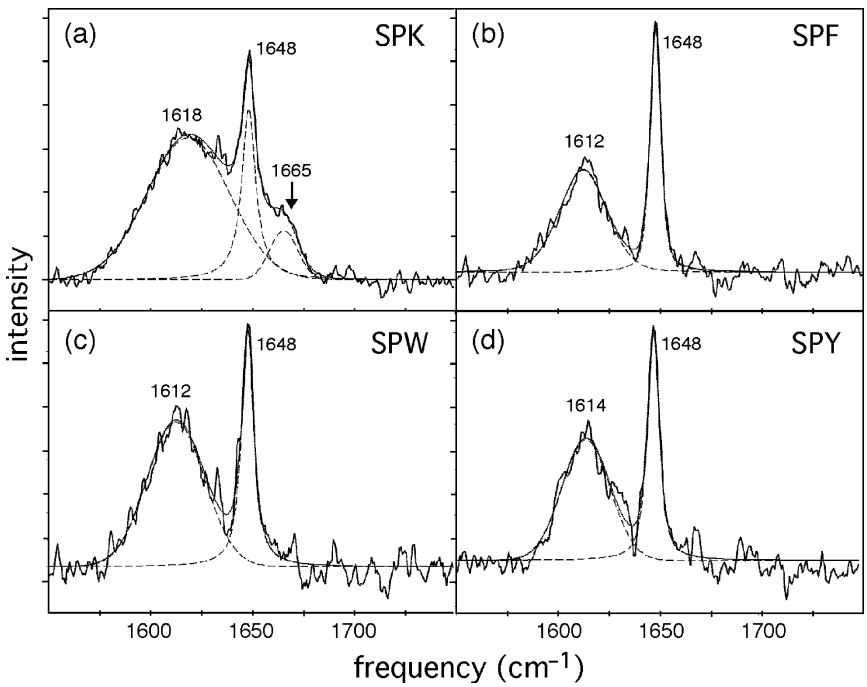

Figure 3 Raman spectra (amide I region, solid lines) of liquid samples of SPK (a), SPF (b), SPW (c) and SPY (d) in the absence of CNTs. Dotted lines represent fitted bands (see Materials and Methods for details).

is typically associated with unordered or turn (e.g. β-turn) structures, whereas the weaker signal below 1615 cm^{-1} is assigned to aromatic residue ring modes. The SPW peptide had a surprisingly poor S/N, which leads to less confidence in the exact positions of the contributing bands (Figure 4(b)); the broad feature at ~1603 cm^{-1} is likely composed of at least two closely spaced bands as seen in SPF and SPY, and the feature

DOI: 10.1002/psc

at 1648 cm^{-1} in SPW could well be similar in position to the 1635 cm^{-1} band (amide I, β-pleated sheet) observed for SPF. Interestingly, an intense signal for each surfactant peptide at 1665 cm^{-1} suggests that they, counter to expectation, do not form ordered (and more folded) secondary structures when dried on the substrate surface. It is unclear if this result indicates that the surfactant peptides (i) do not self-associate (and form a more folded structure) in the dried state, or (ii) are unable to do so because of sample preparation conditions such as drying rate, or the specific type of substrate used.

Sedimentation Equilibrium Studies of Surfactant Peptides in Solution

The lack of concentration-dependent changes in the CD spectra suggests that these peptides exhibit minimal self-association below a concentration of 200 μM in water. Sedimentation equilibrium ultracentrifugation was also used to assess the solution molecular masses of the surfactant peptides at a 100 μM concentration. Sedimentation experiments were conducted at three different speeds. The resulting data for each peptide were then globally fit using two different models: (i) a single homogeneous species model to generate an apparent molecular mass, and (ii) a monomer/nmer equilibrium model to obtain the associated state. The results of the fits are reported in Table 3.

The single species model yielded reasonable fits to the data for SPK, SPW and SPY as judged by the small, random residuals; Figure 5(c) shows the single species fit for SPY as a representative example. For SPF, a less-satisfactory fit is obtained; we observe residuals which are less random and have a slight pattern, with the fits above the data at low-radius values, below the data in mid-radius region and finally above the data again at high-radius values (Figure 5(a)). The apparent molecular mass obtained for each peptide was smaller than the actual molecular mass of a single peptide (Table 3), with large associated error bars also being observed. SPF again stands out with a significantly larger error bar than seen for the other peptides, again suggesting that the quality of its fit is somewhat worse than that for SPK, SPW and SPY. The low molecular masses are likely the result of nonideality arising from steric exclusion or charge–charge repulsive interactions [46–48]. Electrostatic interactions between solutes are usually screened by the addition of a sufficient concentration of a salt such as NaF which can act to screen the charge–charge interactions. A screening salt was intentionally not added in these experiments in order to mimic the peptide solution conditions used to disperse CNTs. Unfortunately, the

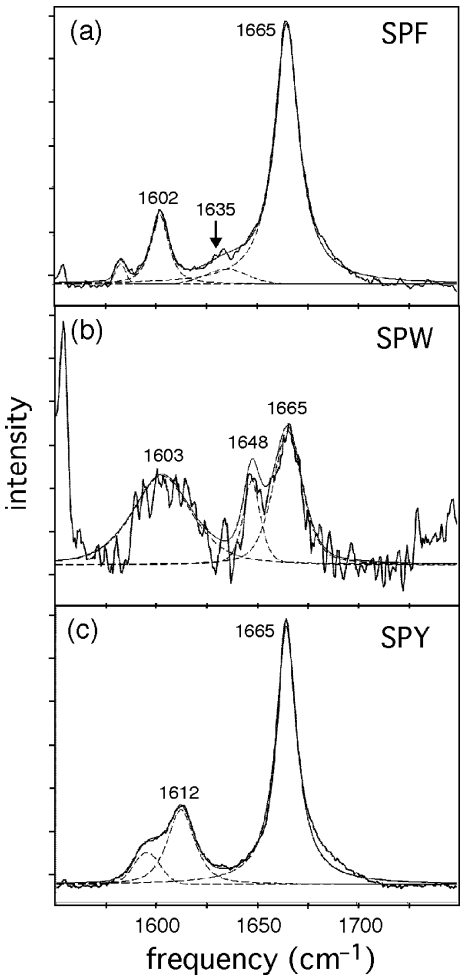

Figure 4 Raman spectra (amide I region, solid lines) of solid samples of SPF (a), SPW (b) and SPY (c) in the absence of CNTs. (see Materials and Methods for details).

Table 3 Results from fits of the sedimentation equilibrium data

Peptide	Single species fit		
	Apparent molecular mass (g mol^{-1})	Expected molecular mass (g mol^{-1})	Monomer/nmer fit Hill Coefficient (n)
SPK	490 ± 250	939	0.26 ± 1.6
SPF	$220 \pm 1.30 \times 10^3$	958	$1.4 \times 10^{-3} \pm 3.7 \times 10^3$
SPW	230 ± 380	997	$7.1 \times 10^{-2} \pm 0.95$
SPY	330 ± 680	974	0.59 ± 0.36

DOI: 10.1002/psc

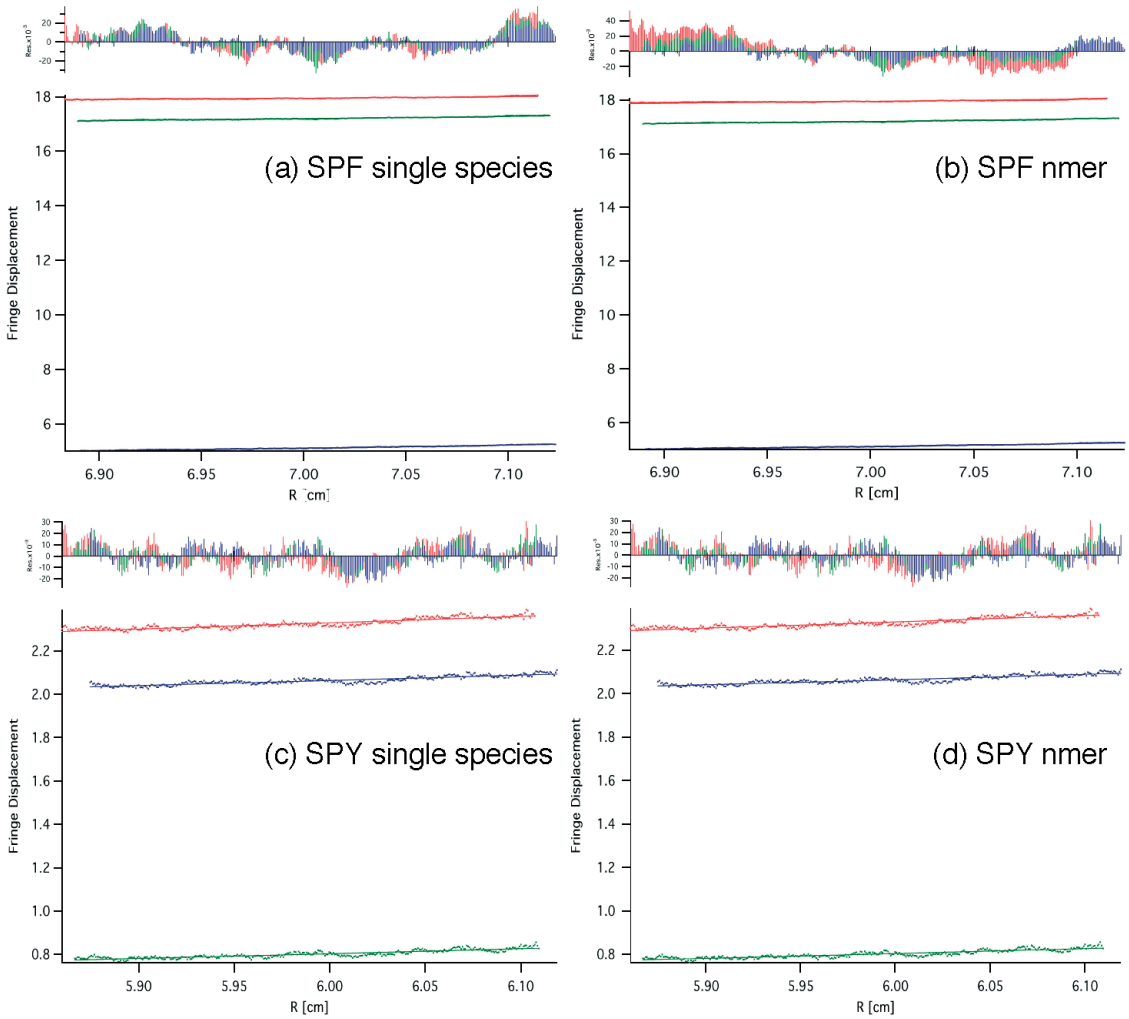

Figure 5 Sedimentation equilibrium ultracentrifugation data and associated fits shown for SPF (a and b); SPY (c and d). See Materials and Methods for details of the single species (a), (c) and monmer/nmer (b), (d) models used. In each panel, the residuals of the fits are shown at the top and the actual data with associated fits shown at the bottom.

low-molecular masses make it difficult to interpret these results from the single species fits.

The monomer/nmer model was also utilized to fit the sedimentation data for each peptide, with the molecular mass fixed, and the Hill Coefficient (n) and dissociation constant allowed to vary for each fit. The resulting fit was deemed reasonable for each peptide with the exception of SPF, which again displayed nonrandom residuals and exceptionally large errors in the fitted value for n (Figure 5(b) and (d)). The values obtained for n for SPW, SPY and SPK were all close to a value of 1 (Table 3), suggesting that these peptides remain largely monomeric in aqueous solution at a concentration of 100 μM.

Taken together, the Raman, CD and sedimentation results indicate that SPW, SPY and SPK are all largely monomeric at 100 μM concentration. This is not surprising, considering the high positive charge originating from the $(Lys)_2$ 'head group' of each peptide; the pH of each peptide solution in water is ~5–6, which is well below the pKa of the Lys side chain, so each Lys residue should be protonated. The results for SPF are less conclusive; however, the similarity in the CD results of SPF with the other three peptides suggest that SPF likely behaves similarly. Since it is important to minimize peptide/peptide interactions while having as much peptide available to interact with the SWNTs for nanotube dispersion, we selected a peptide concentration of 100 μM for use in the peptide/CNT dispersion studies.

Optical Spectroscopy of Surfactant Peptide/SWNT Dispersions

Our motivation for designing the surfactant peptide system was to better understand the interactions of specific aromatic AAs with SWNTs. The stronger the peptide/SWNT interaction, the more peptide that will bind to the surface of the SWNTs and, consequently, the better that the SWNTs will be dispersed. Sonication of SWNTs with each surfactant peptide solution (100 μM

DOI: 10.1002/psc

peptide concentration), followed by centrifugation at 16 000 *g* for 10 min, yielded gray to dark-gray liquid dispersions characteristic of peptide-dispersed CNTs (not shown). Optical spectroscopy was then used to quantify the amount of CNTs dispersed, with the absorbance at 500 nm (A_{500}) used as a measure of the relative concentration of CNTs [2]. Figure 6 compares the CNT content in the four-surfactant peptide/SWNT dispersions after the 16 000 *g*-centrifugation step. SPW displays the highest capability in dispersing CNTs, with more than twice the absorbance as is measured for the SPF or SPY dispersions. SPY and SPF display similar amounts of CNTs dispersed. SPK, in contrast, disperses a negligible amount of CNTs as compared to the SPF, SPY and SPW samples.

Another question we wished to address was how well the various surfactant peptides debundle CNT aggregates. Because of their hydrophobic nature, SWNTs naturally bundle, forming CNT 'ropes' containing multiple individual SWNTs. At a relatively low centrifugation speed (16 000 *g* used above), a CNT dispersion will typically contain a mixture of individual SWNTs and small CNT bundles each containing two to several SWNTs; increasing the centrifugation to at least 50 000 *g* greatly enriches the relative population of individual SWNTs [20]. To address the issue of CNT aggregate debundling by the surfactant peptides, we centrifuged the original 16 000 *g*-dispersions at 100 000 *g* (120 min) and again used UV–Vis–NIR spectroscopy to assess the resulting dispersions. The resulting optical spectra of the surfactant peptide/SWNT dispersions, in general, reveal absorption features in the UV, visible and NIR regions consistent with dispersed CNTs (Figure 7). The SPY and SPW dispersions display multiple sharp, well-separated

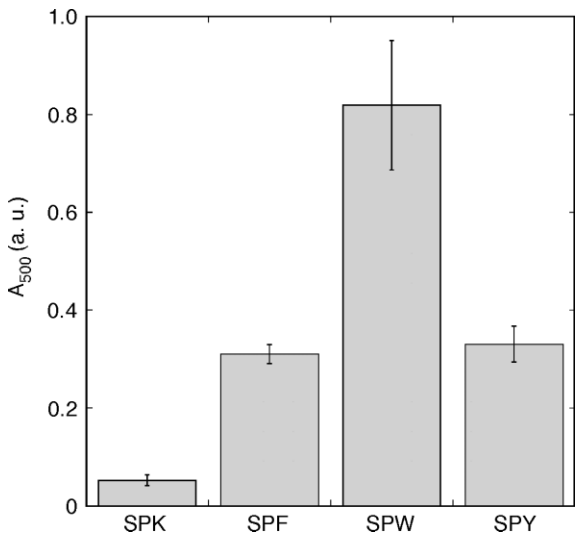

Figure 6 Concentration of CNTs in peptide/SWNT dispersions after 16, 000 *g*-centrifugation step. The absorbance at 500 nm is used as a measure of CNT concentration. Value (and associated error bar) reported for each peptide is the average of three separate experiments.

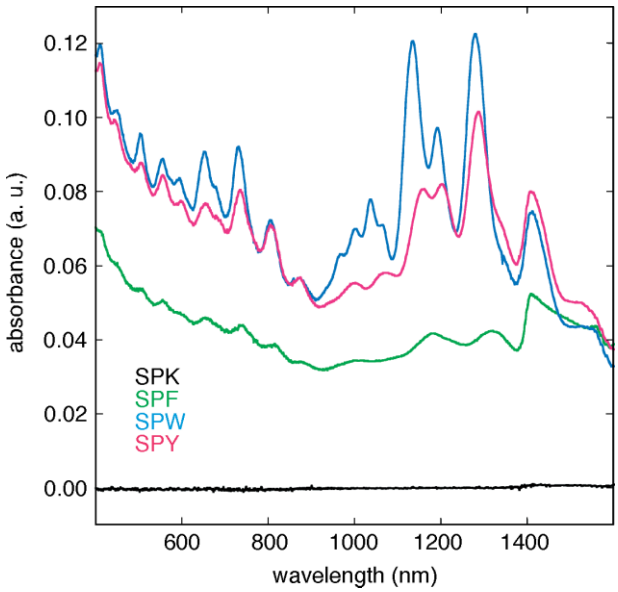

Figure 7 UV–Vis–NIR spectra of peptide/SWNT dispersions after 100, 000 *g*-centrifugation step.

absorption bands. The bands correspond to transitions between van Hove singularities of the SWNTs, with the first van Hove transition (E_{11}) of semiconducting SWNTs between 800 and 1600 nm, E_{22} transitions between 550 and 900 nm, and transitions of metallic SWNTs between 400 and 600 nm [10]. The sharpness of these bands, which depends on the bundling state of SWNTs in the dispersion, suggests that the SWNTs are predominantly isolated. The optical spectrum for the SPF dispersion has a lower overall absorption and less-defined features at all wavelengths as compared to the SPY and SPW dispersions. In contrast to the other three, the SPK dispersion is practically featureless, suggesting that a minimal amount of SWNTs are present. The spectra for SPY, SPW and SPF have a similar number of absorption bands with similar wavelengths, suggesting that the specific SWNT species in each dispersion are similar for the three samples, with the main variation being changes in the relative concentrations of specific SWNT types.

A comparison of A_{500} for the different peptide/SWNT dispersions reveals that the same general absorbance trend is observed at 100 000 *g* that was seen at 16 000 *g* (Figure 8). SPW still disperses the most CNTs, although under these conditions SPY is now able to disperse a comparable amount of CNTs. SPF generates a dispersion with about half the CNT concentration, and SPK is shown to be completely inefficient at dispersing nanotubes. Although the general trend between peptide dispersions is similar at the two centrifugation speeds, an important difference is revealed when, for each peptide, the A_{500} ratio at the two different speeds is compared $[(A_{500})_{16k}/(A_{500})_{100k}]$. Whereas SPF and SPY have similar ratios (0.21 and 0.26, respectively), SPW has a significantly smaller ratio of 0.11, indicating

DOI: 10.1002/psc

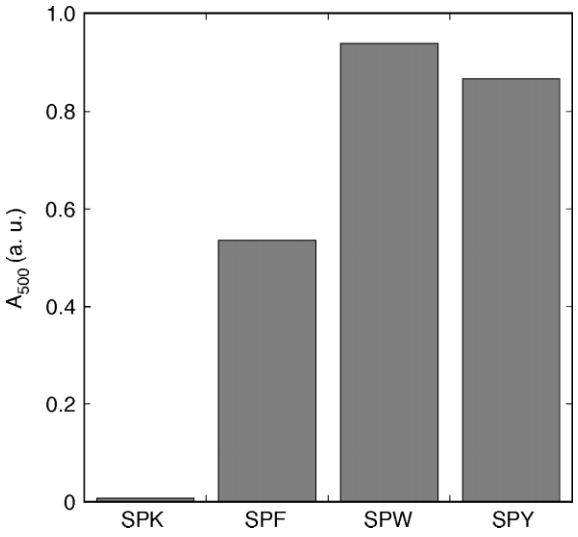

Figure 8 Concentration of CNTs in peptide/SWNT dispersions after 100,000 *g*-centrifugation step. The absorbance at 500 nm is used as a measure of CNT concentration.

that a larger fraction of the dispersed CNTs are removed by the high-speed centrifugation in the SPW dispersion than for the other two peptides. We attribute this difference to an enhanced ability of SPW to disperse CNT bundles *versus* the other peptides. Upon dispersion in the presence of peptide, SWNT bundles are disrupted forming smaller bundles or individual SWNTs. Depending on the coverage of the peptide coating, those CNTs will either be dispersed or precipitate. At low-centrifugation speeds, bundles and individual CNTs stay dispersed as long as they have enough peptide coating, but when a high-speed centrifugation (100 000 *g*) is performed, larger bundles and most small bundles will precipitate, leaving the dispersion containing mostly individual SWNTs. Thus, for a sample with a higher concentration of individual SWNTs, high-speed centrifugation decreases the CNT concentration less than those samples with more bundled SWNTs. The larger decrease in CNT concentration for the SPW dispersion indicates that a larger fraction of CNTs are bundled in the 16 000 *g*-dispersion (stated differently, SPW is nonselective, dispersing both CNT bundles and individual SWNTs); at the high speed, the majority of the bundles are removed from the dispersion, leaving mainly individual SWNTs. In contrast, both SPY and SPF are more selective for individual SWNTs as evidenced by the smaller change in A_{500} observed for those dispersions. The complete loss of SWNTs from the SPK dispersion upon centrifugation at 100 000 *g* indicates that SPK is ineffective at debundling SWNT aggregates.

A general mechanism has been proposed for the debundling and dispersal of CNTs in aqueous solution using sonication and surfactants which provides possible insight into the observed behaviors of the surfactant peptides [49]. In the proposed mechanism, shearing forces from sonication are thought to generate fraying at bundle ends. The newly exposed CNT surfaces then provide locations for the surfactants to adsorb. This process of exfoliation/surfactant adsorption continues until individual CNTs are removed from the bundle. Once coated with surfactant, the individual CNTs are then inhibited from reassociation. As discussed previously, the presence of one or more aromatic groups in a surfactant increases adsorption to CNTs [23,25,26]. In our surfactant peptide system, the larger Trp side chain, with more aromatic surface area, is likely what makes SPW better at dispersing both bundled and individual CNTs at 16 000 *g*. The effectiveness of a surfactant at debundling CNTs, however, should also be related to its ability to intercalate between CNTs at the frayed ends of a bundle. The results presented in this work suggest that the smaller aromatic side chain in Tyr and Phe (as compared to Trp) give SPY and SPF an advantage at intercalation and debundling. The additional hydroxyl group in Tyr makes this peptide slightly more polar than SPF. Intercalation of SPY should make the frayed opening more polar and, therefore, disfavor CNT/CNT reassociation and allow further insertion of additional peptides and solvent.

Raman Spectroscopy of Surfactant Peptide/SWNT Dispersions

Raman spectroscopy is a method which has been utilized extensively to characterize CNT-based dispersions and solid-state materials [50–57]. In the low wavenumber region (from 150 to 350 cm^{-1}), a prominent feature observed for CNTs is the radial breathing mode, which is associated with a symmetric expansive and contractive movement of all carbon atoms in the radial direction; peaks in this region indicate the presence of a particular population of CNTs [52,58]. The diameter of a given SWNT is inversely related to the frequency of its observed RBM. At a particular excitation wavelength, the (n,m) of the SWNTs in resonance can be identified directly [59,60], where n and m are the roll up vector integers that identify a nanotube's specific chirality and diameter [58]. Figure 9(a) shows the Raman spectra (633 nm excitation) of the same SPF/SWNT, SPY/SWNT and SPW/SWNT dispersions used for optical absorption measurements, with all spectra normalized to the G-line feature at ~1590 cm^{-1}. The three spectra show similar SWNT-based resonances, including those in the RBM region, the D-band at ~1310 cm^{-1} and the G-band at ~1591 cm^{-1} [55,61,62]. The comparison of the RBM region for each peptide/SWNT dispersion (Figure 9(b)) indicates that each dispersion contains similar SWNT populations that are resonant with the 633-nm incident laser. These Raman spectra are similar to those for a raw HiPco SWNT sample (data not shown) and for previous SDS dispersions of HiPco SWNTs [63], suggesting that the surfactant peptides do not display

DOI: 10.1002/psc

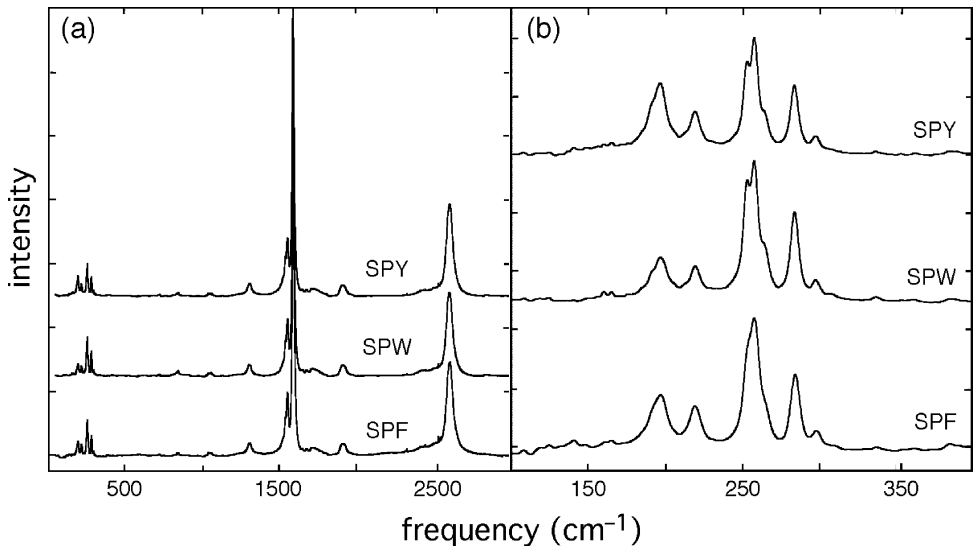

Figure 9 Raman spectra of peptide/SWNT dispersions (633 nm excitation). (a) full spectra, (b) RBM regions.

dispersion selectivity. Similar results are also seen for Raman spectra collected with 488-nm excitation of the SPF/SWNT, SPY/SWNT and SPW/SWNT dispersions (Figure 10). Taken together, the Raman results indicate that the surfactant peptides SPF, SPY and SPW disperse similar types of SWNTs.

Phosphate-induced Peptide/SWNT Self-Assembly

Interestingly, the surfactant peptides exhibit a tendency to self-assemble when KH_2PO_4 is added to the peptide solution to buffer the pH. Figure 11 compares the CD spectra of each peptide in DI water *versus* phosphate buffer (pH 5). For SPF, a slight precipitate slowly forms when phosphate buffer is used to dissolve the peptide. Consistent with this is the significant decrease which is observed in the overall intensity of the CD spectrum in the presence of phosphate, again suggestive of a loss of peptide. SPY shows a slight change in secondary structure with phosphate, with a small negative feature evident at ~215 nm, indicative of the formation of β-sheet secondary structure. In contrast, no structural change was observed for SPW. The precipitation of SPF and the phosphate-induced folding of SPY are consistent with peptide aggregation. It should be noted that the pH of the peptide solutions without buffer is already between 5 and 6, which indicates that it is the addition of the phosphate salt that likely promotes peptide self-assembly and not a change in pH.

The addition of phosphate also leads to the formation of interesting peptide/SWNT architectures upon drying. Figure 12(a) and (b) show SEM images of the SPF/SWNT dispersion upon drying on SEM grids in the absence and presence of phosphate, respectively. In the absence

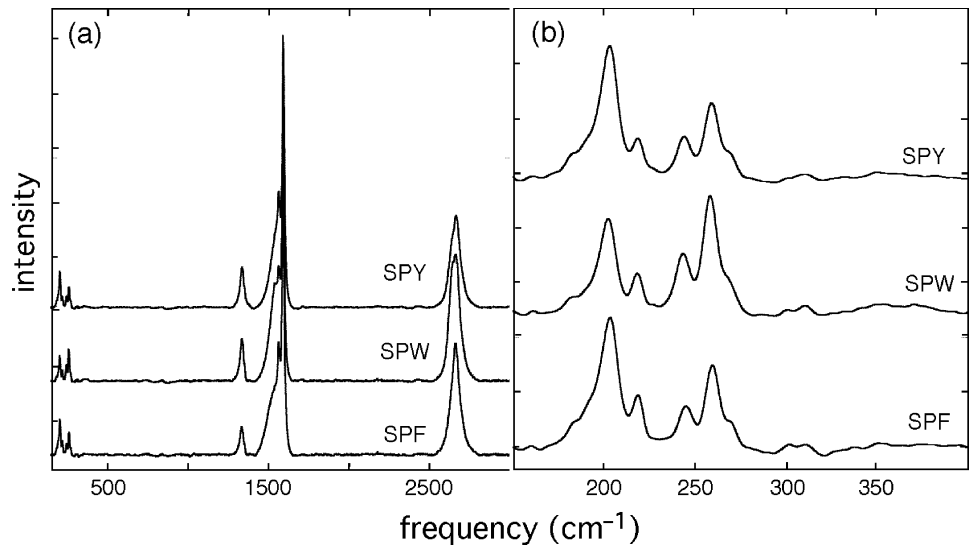

Figure 10 Raman spectra of peptide/SWNT dispersions (488-nm excitation). (a) full spectra, (b) RBM regions.

DOI: 10.1002/psc

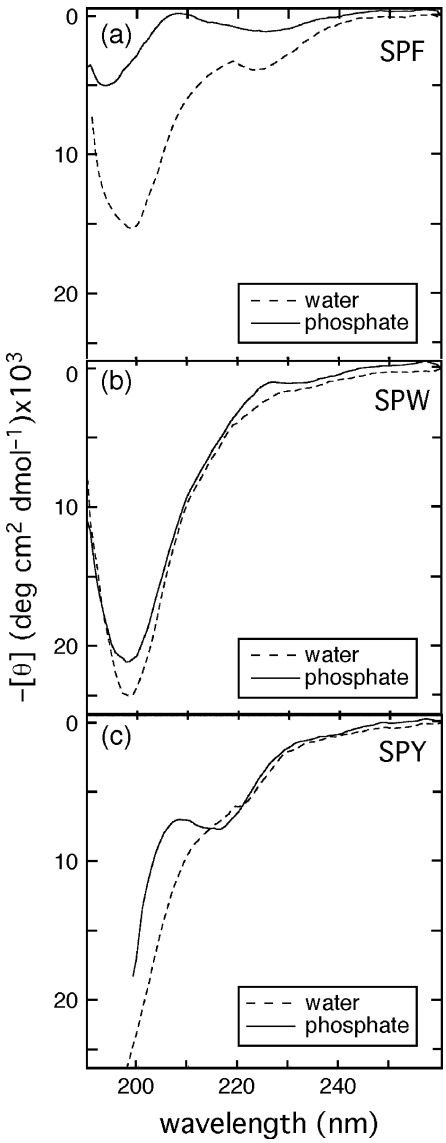

Figure 11 CD spectra of 100 μM SPF (a), SPW (b) and SPY (c) in water and phosphate buffer in the absence of CNTs.

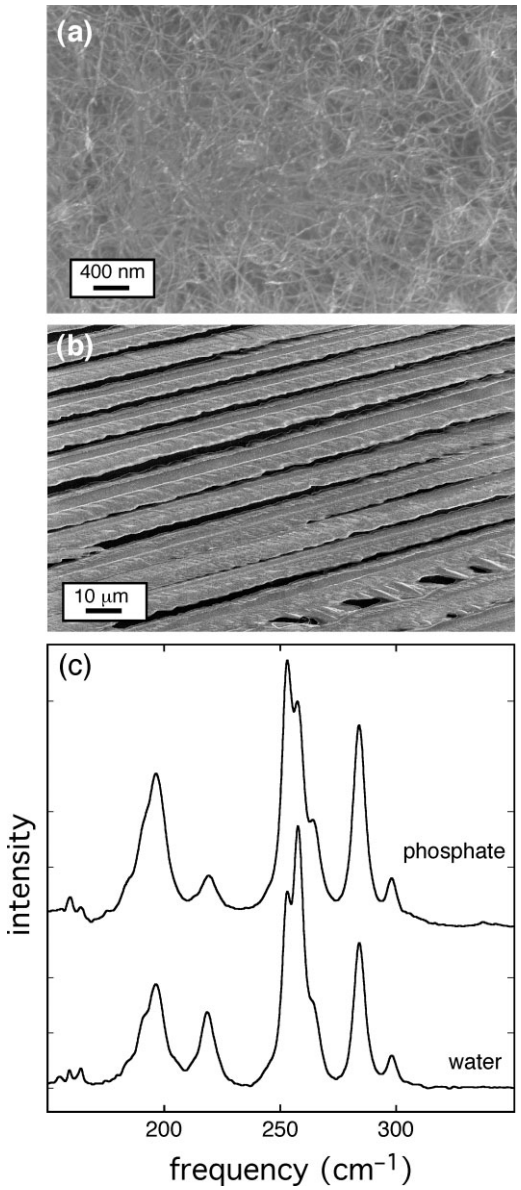

Figure 12 (a) SEM image of SPF/SWNT dispersion in water; (b) SEM image of SPF/SWNT dispersion in phosphate buffer; (c) RBM region of Raman spectra of SPF/SWNT dispersions (633-nm excitation).

of phosphate, the dispersion dries to form only small bundles of peptide-coated SWNTs (Figure 12(a)), similar to those seen before in our laboratory for other peptide/SWNT systems [19,21]. In the presence of phosphate buffer, however, we observe fibrous structures that form upon drying, suggesting that the self-assembly of SPF tends to promote the formation of these organized SPF/SWNT structures (Figure 12(b)). A control experiment was also conducted with SPF plus phosphate buffer solution (no SWNTs) dropped on the same grid; no fibrous structures were observed. Figure 12(c) shows the Raman spectra (RBM region) of the SPF/SWNT solid samples (Figure 12(a) and (b)). The two solid samples give similar RBM Raman spectra, implying that the formation of the organized SPF/SWNT structures is not due to dispersion of different types of SWNTs, but is instead due to the phosphate-induced peptide self-assembly. The negatively charged phosphate ion is likely acting by screening the positive head groups of the surfactant peptides, allowing them to self-associate.

Similar experiments were performed using SPW and SPY. Solid-peptide/SWNT structures were also observed when phosphate buffer was present in the other peptide/SWNT dispersions (not shown) However, the solid structures formed by the SPY and SPW dispersions were not as ordered as that observed for SPF, which we attribute to the fact that under the same experimental conditions, phosphate induces more peptide self-assembly in SPF than in SPW or SPY.

DOI: 10.1002/psc

CONCLUSIONS

A series of surfactant peptides were designed to build a system which can test the affinity of different AAs for SWNTs. Among the three tested aromatic AAs, Trp is best at dispersing all SWNTs, including both bundled and individual SWNTs. Both SPF and SPY are more selective for individual SWNTs. Optical and Raman spectra reveal that the specific SWNT species dispersed by each peptide are the same, with small differences observed in the populations of certain types of SWNTs. Surfactant peptides were also found to have the potential of being scaffolds to induce self-assembly of the peptide/SWNT composites.

Acknowledgements

We are grateful for insightful discussions with James Lear. This work was supported by a grant from the Human Frontier Science Program (GRD; grant RGY0070/2005-C).

REFERENCES

1. Dresselhaus MS, Dresselhaus G, Avouris P (eds). *Carbon Nanotubes: Synthesis, Structure, Properties, and Applications*, Vol. 80. Springer: New York, 2001.
2. Bahr JL, Mickelson ET, Bronikowski MJ, Smalley RE, Tour JM. Dissolution of small diameter single-wall carbon nanotubes in organic solvents? *Chem. Commun.* 2001; 193–194.
3. Niyogi S, Hamon MA, Hu H, Zhao B, Bhowmik P, Sen R, Itkis ME, Haddon RC. Chemistry of single-walled carbon nanotubes. *Acc. Chem. Res.* 2002; **35**: 1105–1113.
4. Sinnott SB. Chemical functionalization of carbon nanotubes. *J. Nanosci. Nanotechnol.* 2002; **2**: 113–123.
5. Sun Y-P, Fu K, Lin Y, Huang W. Functionalized carbon nanotubes: properties and applications. *Acc. Chem. Res.* 2002; **35**: 1096–1104.
6. Bahr JL, Tour JM. Covalent chemistry of single-wall carbon nanotubes. *J. Mater. Chem.* 2002; **12**: 1952–1958.
7. Hirsch A. Functionalization of single-walled carbon nanotubes. *Angew. Chem. Int. Ed. Engl.* 2002; **41**: 1853–1859.
8. Boul PJ, Liu J, Mickelson ET, Huffman CB, Ericson LM, Chiang IW, Smith KA, Colbert DT, Hauge RH, Magrave JL, Smalley RE. Reversible sidewall functionalization of buckytubes. *Chem. Phys. Lett.* 1999; **310**: 367–372.
9. Chen J, Hamon MA, Hu H, Chen Y, Rao AM, Eklund PC, Haddon RC. Solution properties of single-walled carbon nanotubes. *Science* 1998; **282**: 95–98.
10. Vigolo B, Penicaud A, Coulon C, Sauder C, Pailler R, Journet C, Bernier P, Poulin P. Macroscopic fibers and ribbons of oriented carbon nanotubes. *Science* 2000; **290**: 1331–1334.
11. O'Connell MJ, Bachilo SM, Huffman CB, Moore VC, Strano MS, Haroz EH, Rialon KL, Boul PJ, Noon WH, Kittrell C, Ma JP, Hauge RH, Weisman RB, Smalley RE. Band gap fluorescence from individual single-walled carbon nanotubes. *Science* 2002; **297**: 593–596.
12. O'Connell MJ, Boul P, Ericson LM, Huffman C, Wang Y, Haroz E, Kuper C, Tour J, Ausman KD, Smalley RE. Reversible water-solubilization of single-walled carbon nanotubes by polymer wrapping. *Chem. Phys. Lett.* 2001; **342**: 265–271.
13. Curran SA, Ajayan PM, Blau WJ, Carroll DL, Coleman JN, Dalton AB, Davey AP, Drury A, McCarthy B, Maier S, Strevens A. A composite from poly(m-phenylenevinylene-co-2,5-dioctoxy-p-phenylenevinylene) and carbon nanotubes: A novel material for molecular optoelectronics. *Adv. Mater.* 1998; **10**: 1091–1094.
14. Tang BZ, Xu HY. Preparation, alignment, and optical properties of soluble poly(phenylacetylene)-wrapped carbon nanotubes. *Macromolecules* 1999; **32**: 2569–2576.
15. Zheng M, Jagota A, Strano MS, Santos AP, Barone P, Chou SG, Diner BA, Dresselhaus MS, Mclean RS, Onoa GB, Samsonidze GG, Semke ED, Usrey ML, Walls DJ. Structure-based carbon nanotube sorting by sequence-dependent DNA assembly. *Science* 2003; **302**: 1545–1548.
16. Zheng M, Jagota A, Semke ED, Diner BA, Mclean RS, Lustig SR, Richardson RE, Tassi NG. DNA-assisted dispersion and separation of carbon nanotubes. *Nat. Mater* 2003; **2**: 338–342.
17. Arnold MS, Guler MO, Hersam MC, Stupp SI. Encapsulation of carbon nanotubes by self-assembling peptide amphiphiles. *Langmuir* 2005; **21**: 4705–4709.
18. Witus LS, Rocha J-DR, Yuwono VM, Paramonov SE, Weisman RB, Hartgerink JD. Peptides that non-covalently functionalize single-walled carbon nanotubes to give controlled solubility characteristics. *J. Math. Chem.* 2007; **17**: 1909–1915.
19. Dieckmann GR, Dalton AB, Johnson PA, Razal J, Chen J, Giordano GM, Munoz E, Musselman IH, Baughman RH, Draper RK. Controlled assembly of carbon nanotubes by designed amphiphilic peptide helices. *J. Am. Chem. Soc.* 2003; **125**: 1770–1777.
20. Zorbas V, Ortiz-Acevedo A, Dalton AB, Yoshida MM, Dieckmann GR, Draper RK, Baughman RH, Jose-Yacaman M, Musselman IH. Preparation and characterization of individual peptide-wrapped single-walled carbon nanotubes. *J. Am. Chem. Soc.* 2004; **126**: 7222–7227.
21. Dalton AB, Ortiz-Acevedo A, Zorbas V, Brunner E, Sampson WM, Collins S, Razal JM, Yoshida MM, Baughman RH, Draper RK, Musselman IH, Jose-Yacaman M, Dieckmann GR. Hierarchical Self-assembly of peptide-coated carbon nanotubes. *Adv. Funct. Mater.* 2004; **14**: 1147–1151.
22. Xie H, Ortiz-Acevedo A, Baughman RH, Draper RK, Musselman IH, Dalton AB, Dieckmann GR. Peptide cross-linking modulated stability and assembly of peptide-wrapped single-walled carbon nanotubes. *J. Mater. Chem.* 2005; **15**: 1734–1741.
23. Zorbas V, Smith AL, Ortiz-Acevedo A, Xie H, Dalton AB, Dieckmann GR, Draper RK, Baughman RH, Musselman IH. Importance of aromatic content for peptides/single-walled carbon nanotube interactions. *J. Am. Chem. Soc.* 2005; **127**: 12323–12328.
24. Mclachlan AD, Stewart M. Tropomyosin Coiled-Coil Interactions–evidence for an Unstaggered structure. *J. Mol. Biol.* 1975; **98**: 293–304.
25. Islam MF, Rojas E, Bergey DM, Johnson AT, Yodh AG. High weight fraction surfactant solubilization of single-wall carbon nanotubes in water. *Nano Lett.* 2003; **3**: 269–273.
26. Chen RJ, Zhang Y, Wang D, Dai H. Noncovalent sidewall functionalization of single-walled carbon nanotubes for protein immobilization. *J. Am. Chem. Soc.* 2001; **123**: 3838–3839.
27. Oakley MG, Hollenbeck JJ. The design of antiparallel coiled coils. *Curr. Opin. Struct. Biol.* 2001; **11**: 450–457.
28. Yu YB. Coiled-coils: stability, specificity, and drug delivery potential. *Adv. Drug Deliv. Rev.* 2002; **54**: 1113–1129.
29. Lupas AN, Gruber M. The structure of alpha-helical coiled coils. In *Fibrous Proteins: Coiled-coils, Collagen and Elastomers*, Vol. 70, Parry DAD, Squire P (eds). Academic Press: St Louis, Missouri, 2005; 37–79.
30. Sreerama N. Software and related literature located at the website http://lamar.colostate.edu/~sreeram/CDPro. [Last accessed: November 2007].
31. Cohn EJ, Edsall JT. *Proteins, Amino Acids, and Peptides as Ions and Dipolar Ions*. Hafner Publishing: New York, 1965.
32. Laue TM, Shah BD, Ridgeway TM, Pelletier SL. Computer aided interpretation of analytical sedimentation data for proteins. In *Analytical Ultracentrifugation in Biochemistry and Polymer Science*,

Harding S, Rowe A, Horton J (eds). Royal Society of Chemistry: Cambridge, 1992; 90–125.
33. Peticolas WL. Raman spectroscopy of DNA and proteins. *Methods in Enzymology*, Vol. 246. Academic Press: San Diego, CA, 1995; 389–416.
34. Tu AT. *Raman Spectroscopy in Biology: Principles and Applications*. John Wiley and Sons: New York, 1982.
35. Jung C. Insight into protein structure and protein-ligand recognition by Fourier transform infrared spectroscopy. *J. Mol. Recognit.* 2000; **13**: 325–351.
36. Ismail AA, Mantsch HH, Wong PTT. Aggregation of chymotrypsinogen: portrait by infrared spectroscopy. *Biochim. Biophys. Acta* 1992; **1121**: 183–188.
37. Panick G, Malessa R, Winter R. Differences between the pressure- and temperature-induced denaturation and aggregation of b-lactoglobulin A, B and AB monitored by FT-IR spectroscopy and small-angle X-ray scattering. *Biochemistry* 1999; **38**: 6512–6519.
38. Pelton JT, McLean LR. Spectroscopic methods for analysis of protein secondary structure. *Anal. Biochem.* 2000; **277**: 167–176.
39. Zheng R, Zheng X, Dong J, Carey PR. Proteins can convert to b-sheet in single crystals. *Prot. Sci.* 2004; **13**: 1288–1294.
40. Benaki DC, Aggeli A, Chryssikos GD, Yiannopoulos YD, Kamitsos EI, Brumley E, Case ST, Boden N, Hamodrakas S. Laser-Raman and FT-IR spectroscopic studies of peptide-analogues of silkmoth chorion protein segments. *Int. J. Biol. Macromol.* 1998; **23**: 49–59.
41. Pauthe E, Dauchez M, Mejri M, Berjot M, Mathlouthi M, Larreta-Garde V, Alix AJP. Structural studies of a small (linear, cyclic) peptide as a synthetic substrate for thermolysin. *J. Mol. Struct.* 1999; **480–481**: 423–426.
42. Kim SK, Kim MS, Suh SW. Surface-enhanced Raman Scattering (SERS) of aromatic amino acids and their glycyl dipeptides in silver sol. *J. Raman Spectrosc.* 1987; **18**: 171–175.
43. Forbes RT, Barry BW, Elkordy AA. Preparation and characterisation of spray-dried and crystallised trypsin: FT-Raman study to detect protein denaturation after thermal stress. *Eur. J. Pharm. Sci.* 2007; **30**: 315–323.
44. Chikishev AY, Lucassen GW, Koroteev NL, Otto C, Grevet J. Polarization sensitive coherent anti-Stokes Raman scattering spectroscopy of the amide I band of proteins in solutions. *Biophys. J.* 1992; **63**: 976–985.
45. Jackson M, Haris PI, Chapman D. Conformational transitions in poly(L-lysine)–studies using Fourier transform infra-red spectroscopy. *Biochim. Biophys. Acta* 1989; **998**: 75–79.
46. Waldner JC, Lahr SJ, Edgell MH, Pielak GJ. Nonideality and protein thermal denaturation. *Biopolymers* 1999; **49**: 471–479.
47. Behlke J, Ristau O. Analysis of the thermodynamic non-ideality of proteins by sedimentation equilibrium experiments. *Biophys. Chem.* 1999; **76**: 13–23.
48. Tanford C. *Physical Chemistry of Macromolecules*. John Wiley and Sons: New York, 1961.
49. Strano MS, Moore VC, Miller MK, Allen MJ, Haroz EH, Kittrell C, Hauge RH, Smalley RE. The role of surfactant adsorption during Ultrasonication in the dispersion of single-walled carbon nanotubes. *J. Nanosci. Nanotechnol.* 2003; **3**: 81–86.
50. Yu ZH, Brus LE. (n,m) Structural assignments and chirality dependence in single-wall carbon nanotube Raman scattering. *J. Phys. Chem. B* 2001; **105**: 6831–6837.
51. Brown SDM, Jorio A, Corio P, Dresselhaus MS, Dresselhaus G, Saito R, Kneipp K. Origin of the Breit-Wigner-Fano lineshape of the tangential G-band feature of metallic carbon nanotubes. *Phys. Rev., B* 2001; **63**: 155414(1)–155414(8).
52. Sauvajol JL, Anglaret E, Rols S, Alvarez L. Phonons in single wall carbon nanotube bundles. *Carbon* 2002; **40**: 1697–1714.
53. Souza AG, Jorio A, Swan AK, Unlu MS, Goldberg BB, Saito R, Hafner JH, Lieber CM, Pimenta MA, Dresselhaus G, Dresselhaus MS. Anomalous two-peak G '-band Raman effect in one isolated single-wall carbon nanotube. *Phys. Rev., B* 2002; **65**: 085417(1)–085417(8).
54. Saito R, Grueneis A, Cancado LG, Pimenta MA, Jorio A, Dresselhaus G, Dresselhaus MS, Souza AG. Double resonance Raman spectra in disordered graphite and single wall carbon nanotubes. *Mol. Cryst. Liq. Cryst.* 2002; **387**: 287–296.
55. Dresselhaus MS, Dresselhaus G, Jorio A, Souza AG, Saito R. Raman spectroscopy on isolated single wall carbon nanotubes. *Carbon* 2002; **40**: 2043–2061.
56. Dresselhaus MS, Jorio A, Dresselhaus G, Saito R, Souza AG, Pimenta MA. Raman spectroscopy of nanoscale carbons and of an isolated carbon nanotube. *Mol. Cryst. Liq. Cryst.* 2002; **387**: 245–253.
57. Kuzmany H, Pfeiffer R, Hulman M, Kramberger C. Raman spectroscopy of fullerenes and fullerene-nanotube composites. *Philos. Trans. R. Soc. Lond. A* 2004; **362**: 2375–2406.
58. Saito R, Dresselhaus G, Dresselhaus MS. *Physical Properties of Carbon Nanotubes*. Imperial College Press: London, 1998.
59. Bachilo SM, Strano MS, Kittrell C, Hauge RH, Smalley RE, Weisman RB. Structure-assigned optical spectra of single-walled carbon nanotubes. *Science* 2002; **298**: 2361–2366.
60. Strano MS. Probing chiral selective reactions using a revised Kataura plot for the interpretation of single-walled carbon nanotube spectroscopy. *J. Am. Chem. Soc.* 2003; **125**: 16148–16153.
61. Alvarez WE, Pompeo F, Herrera JE, Balzano L, Resasco DE. Characterization of single-walled carbon nanotubes (SWNTs) produced by CO disproportionation on Co-Mo catalysts. *Chem. Mater.* 2002; **14**: 1853–1858.
62. Resasco DE, Herrera JE. Structural characterization of single-walled carbon nanotubes. In *Encyclopedia of Nanoscience and Nanotechnology*, Vol. 10. American Scientific Publishers: Valencia, CA, 2004; 125–147.
63. Ortiz-Acevedo A, Xie H, Zorbas V, Sampson WM, Dalton AB, Baughman RH, Draper RK, Musselman IH, Dieckmann GR. Diameter-selective solubilization of single-walled carbon Nanotubes by reversible cyclic peptides. *J. Am. Chem. Soc.* 2005; **127**: 9512–9517.
64. Byler D-M, Susi H. Examination of the secondary structure of proteins by deconvolved FTIR spectra. *Biopolymers* 1986; **25**: 469–487.
65. Surewicz WK, Mantsch HH, Chapman D. Determination of protein secondary structure by Fourier transform infrared spectroscopy: a critical assessment. *Biochemistry* 1993; **32**: 389–394.
66. Bandekar J, Krimm S. Vibrational analysis of peptides, polypeptides and proteins: characteristic amide bands of β-turns. *Proc. Natl. Acad. Sci. U.S.A.* 1979; **76**: 774–777.
67. Parker FS. *Applications of Infrared, Raman, and Resonance Raman Spectroscopy in Biochemistry*. Plenum: New York, 1983.